Geophys. J. Int. (1993) **115,** 168–182

Laterally varying reflector at the top of *D″* beneath northern Siberia

S. Houard and H-C. Nataf

Département Terre-Atmosphère-Océan, Ecole Normale Supérieure, 24 rue Lhomond, 75231 Paris cedex 05, France

Accepted 1993 March 4. Received 1993 March 2; in original form 1992 October 30

SUMMARY

We analyse *P*-wave data from the French 'Laboratoire de Détection et Géophysique' (L.D.G) network of digital short-period seismic stations. Whereas our previous paper (Houard & Nataf 1992) showed a few promising Kuril events and depicted the methods we proposed to apply, an extensive analysis of 32 earthquakes from the Kuril/Kamchatka region has now been carried out. By using the deconvolution technique previously described (Houard & Nataf 1992), clear and quantitative evidence of intermediate arrivals between the *P* and *PcP* waves is shown, in the 75–82° distance range. Our approach is complementary to previous studies in the same region, which used broad-band data recorded at a dense narrow-aperture array (Weber & Davis 1990; Weber 1993) or long-period data recorded at the WWSSN stations (Gaherty & Lay 1992). For each station, record sections of deconvolved signals from different earthquakes are built, and lead us to eliminate crustal reverberations beneath L.D.G stations as a major explanation for these secondary arrivals. A compilation of the most conclusive signals has been made. It is perhaps one of the most complete *PdP*-wave record sections, since the move out with distance can be followed clearly with a good sampling over more than 5°. The move out with distance of this extra '*PdP*' arrival, its residual slowness value, eliminates source complexities, diffraction, or multipathing through the Kuril subduction slab as possible explanations. The extra arrivals indicate the existence of a lower mantle reflector. The structure of the 'Lay discontinuity' is investigated, using $T_{PdP}-T_P$ residual traveltimes. Two different residual time versus distance tendencies are found, which correlate to different geographical bounce point regions, indicating the existence of lateral variations of the structure. The *D″* region is also sampled further south at distances well beyond the theoretical triplication cross-over by analysing events from the Honshu/Ryukyu Islands region, but only one *P*-wave branch is observed. The hodochrones and $p-\Delta$ curves of the first *P* arrival are used as a complementary analysis. The global PREM model (Dziewonski & Anderson 1981), predicts correct *P* wave slownesses, though its smooth lower mantle structure does not account for *PdP* observations. This may be an indication that the 'Lay discontinuity' is a global feature. However, the hodochrones of the first *P* arrival do not allow us to test the existence of the discontinuity in the 82–85° cross-over distance range.

Key words: mantle discontinuities, *P* waves, Siberia.

INTRODUCTION

Lay & Helmberger (1983 a and b) were the first to interpret abnormal arrivals between *S* and *ScS* waves in the 75–85° epicentral distance range as reflections from a first-order discontinuity, some 200–300 km above the core–mantle boundary, at the top of the so-called *D″* region. However, three different spherical models were required, one for each sampled region, to fit their whole data set. Ever since then, the study of the *D″* structure has been enhanced, and many authors support the existence of a first-order discontinuity at its top (Zhang & Lay 1984; Young & Lay 1987; Garnero,

Helmberger & Engen 1988; Baumgardt 1989; Weber & Davis 1990; Weber 1993; Young & Lay 1990; Houard & Nataf 1992). However, several features remain puzzling: (1) the discontinuity would not be present everywhere on the globe (Schlittenhardt, Schweitzer & Müller 1985; Garnero *et al.* 1988; Weber & Davis 1990). (2) Its depth can vary by up to 100 km (Lay 1989; Weber & Körnig 1992). (3) For a given earthquake, the reflected wave is not observed at all the stations of a network (Gaherty & Lay 1992). All these characteristics suggest the existence of lateral variations in the structure of *D''*, which is indeed a crucial point to infer geodynamical consequences. An alternative interpretation of these abnormal arrivals, by Haddon & Buchbinder (1986), supports a scattering mechanism on small-scale heterogeneities at the base of the mantle.

If lateral variations exist, then the 1-D model interpretation is somewhat limited, and efforts should be concentrated on the density of observations first, in order to derive accurate 2-D or 3-D structures. Many studies involve waves that travel from the Kuril/Sea-of-Okhotsk/Kamtchatka seismic region, to European stations. Gaherty & Lay (1992) used long-period data from the sparse WWSSN network, whereas Weber & Davis (1990) and Weber (1993) used the regional GRF array, equiped with broad-band instruments. Our study is quite complementary to the previous ones: we analyse *P*-wave data from earthquakes in the Sea-of-Okhotsk/Kamchatka region, recorded on the short-period digital 'Laboratoire de Détection et Géophysique' (L.D.G) network in France. Dense and wide, it is particularly well suited for investigating the deep mantle structure on a 100–1000 km scale.

In a first step, clear observations of anomalous *PdP* waves, between *P* and *PcP*, are presented. They are extensively based on a deconvolution technique described in our previous paper (Houard & Nataf 1992). Only a lower mantle origin is compatible with all the observations. The interpretation is based on *PdP–P* traveltime residuals, and the hodochrones of the first *P*-wave arrival are used as a supplementary constraint. The complex observations cannot be modelled by a single *D''* radial structure beneath northern Siberia. Limits can be set on the velocity gradient above the discontinuity and on the depth of the discontinuity itself. Two traveltime residual tendencies are determined, which are correlated to distinct bounce point regions, and confirm the existence of lateral variations.

THE L.D.G NETWORK

The seismic network run by the L.D.G of the French Atomic Energy Comission (C.E.A) has been described in detail in our previous paper. Fig. 1 shows the location of the stations. The total displacement response of the instrument is inserted in the top right, and compared with that of the WWSSN short-period instrument. The L.D.G network appears to be well suited for investigating deep mantle structure on the 100–1000 km scale. Especially important are: (1) the extension of the network, as will be illustrated in the deconvolution technique, (2) the density of the network, if we consider the great variability of short-period signals from one station to another.

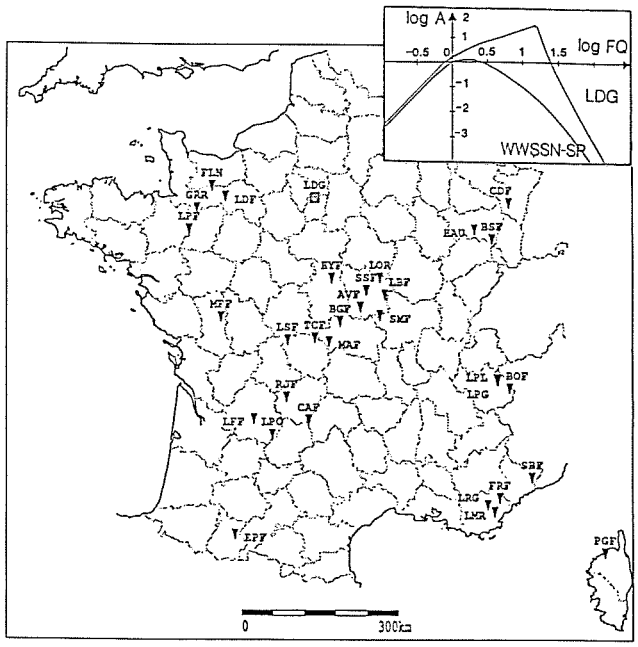

Figure 1. Map of the French seismic L.D.G network. It consists of about 30 permanent short-period stations equipped with the same vertical-component seismograph. The insert at the top right of the figure displays both L.D.G. and WWSSN short-period displacement instrument responses. The L.D.G response is characterized by a maximum of sensitivity around 12 Hz, far beyond that of the classical WWSSN–SP instrument.

Data

Previous studies (Lay & Helmberger 1983 a and b; Weber & Davis 1990; Weber 1993) have shown that extra arrivals between *P* and *PcP*, or *S* and *ScS*, could best be observed in the 70–85° distance range from the epicentre. Three major seismic regions are found in the correct distance range from the L.D.G network: the sea-of-Okhotsk/Kamchatka, the Central America and the Alaska/Aleutians regions. Other criteria have also been applied in the data selection, (1) earthquakes shallower than 50 km have been eliminated, in order to avoid interferences between direct and free-surface reflected waves, (2) magnitudes between 5.4 and 6.0 were selected; large magnitudes usually give complex *P* coda wave trains, rending anomalous arrivals almost undetectable; small magnitudes yield low signal-to-noise ratios, rending again the detectability more than difficult, (3) we have also eliminated events with adequate magnitude, but with a source half-duration longer than 4 s.

As a result, the sea of Okhotsk/Kamchatka region has provided the widest set of accurate data, and especially a very good epicentral distance sampling, even for a given station in the L.D.G network. This last argument will be important to reject crustal reverberations as the origin of the abnormal arrivals. Thus, as a first step, we have concentrated our efforts on this region, with waves bottoming in the lower mantle below the Novaya Zemlya Island, in northern Siberia. Our final data set consists of 32 events. They are listed in Table 1.

Table 1. Kuril Islands/Kamchatka seismic region.

n°	date (y/m/d)	time (h:mn:s)	lat (deg)	long (deg)	depth (km)	mb	$TS_{1/2}^{*}$ (sec)	region	tendency	Source
45	83/04/04	19:04:22.1	52.9	159.8	52.	5.9	3.4	Kamtchatka	NONE	ISC
1	83/04/11	15:34:55.	44.3	147.7	97.	5.7		Kuriles		USGS
46	83/04/15	14:51:58.0	53.4	160.3	56.	5.8	2.0	Kamtchatka	LAY	ISC
3	83/07/24	23:07:32.	53.9	158.4	180.	6.1		Kamtchatka	LAY	USGS
48	83/08/05	00:33:47.5	52.9	159.7	61.	5.4	4.0	Kamthatka	LAY	ISC
8	83/12/08	13:50:51.	46.3	150.9	98.	5.5		Kuriles	NONE	USGS
10	84/02/01	07:28:27.	49.0	146.6	573.	6.0		Okhotsk	INT	USGS
51	84/02/05	18:41:11.6	55.6	161.7	81.	5.3	1.5	Kamtchatka	INT	ISC
12	84/04/20	06:31:10.	50.0	149.0	582.	6.0		Okhotsk	INT	USGS
52	84/06/18	13:06:45.1	52.9	159.4	52.	5.3		Kamtchatka	LAY(+)	ISC
53	84/07/23	15:13:26.4	49.6	155.8	71.	5.3		Kamtchatka	NONE	ISC
14	85/02/23	08:24:07.	47.3	145.7	422.	5.3		Okhotsk	NONE	USGS
54	85/04/03	08:18:09.2	51.9	158.7	52.	5.4	2.3	Kamtchatka	NONE	ISC
55	85/05/19	08:07:47.0	53.6	160.5	54.	6.0	3.1	Kamtchatka	NONE	ISC
15	85/10/18	04:19:08.	46.0	146.0	271.	6.0		Kuriles	NONE	USGS
57	86/02/19	10:54:45.6	48.5	153.4	110.	5.3	1.6	Kuriles		ISC
58	86/03/02	03:14:43.2	51.6	156.9	131.	5.5	2.5	Kamtchatka	LAY(+)	ISC
59	86/06/17	00:42:38.2	53.9	160.4	57.	5.7	2.0	Kamtchatka	INT(+)	ISC
16	86/07/19	05:59:37.	47.	151.0	141.	5.9		Kuriles	NONE	USGS
60	87/05/12	04:03:59.8	49.9	156.3	54.	5.4		Kuriles	NONE	ISC
25	87/07/08	22:56:02.	46.4	149.4	152.	5.4		Kuriles	INT	USGS
61	87/07/11	05:13:13.0	50.2	156.2	55.	5.4	1.7	Kuriles	NONE	ISC
26	87/07/14	23:46:04.	49.6	147.8	576.	5.6		Okhotsk	INT	USGS
28	87/09/23	07:15:43.	46.	149.5	131.	5.9		Kuriles	INT(+)	USGS
31	88/02/19	22:37:11.	52.8	158.2	120.	5.2		Kamtchatka	LAY	USGS
34	88/06/26	09:23:00.	46.3	144.1	327.	5.2		Okhotsk	INT	USGS
63	89/08/30	11:38:12.7	55.6	161.4	73.	5.7	2.3	Kamtchatka	INT(+)	ISC
64	89/09/15	18:34:13.0	53.2	159.7	52.	5.5	2.1	Kamtchatka	LAY(+)	ISC
65	90/03/10	10:15:03.9	50.9	157.2	51.	5.7	2.1	Kamtchatka	LAY	USGS
66	90/10/16	06:13:13.7	49.0	155.1	83.	6.0	3.0	Kuriles	NONE	USGS
67	91/01/10	13:57:19.8	51.5	157.3	70.	5.4		Kuriles	NONE	USGS
68	91/04/08	13:34:04.5	52.4	157.9	145.	5.6	2.4	Kamtchatka	INT	USGS

Earthquakes' parameters from the U.S.G.S. preliminary determination of epicentres (P.E.D.) or ISC bulletins.
*: Source half-durations are from P.D.E. bulletins.
Earthquakes with the 'best observations' of *PdP* (see text) are indicated by a cross in the 'tendency' column.

CLEAR OBSERVATIONS OF ABNORMAL WAVES

In a previous paper (Houard & Nataf 1992), we have shown signals for a few Kuril earthquakes recorded on the L.D.G that presented anomalous arrivals at some stations of the network. In this paper, an extensive analysis of 32 earthquakes is carried out, and quantitative results are given. Our most conclusive event, the 1986 March 2 Kamchatka event, is shown, in Fig. 2(a). In a $T-\Delta$ plot, the signals have been time shifted so as to be aligned on the theoretical *P* arrival. The times at the bottom apply to the station closest to the epicentre (CDF). Also marked are the theoretical traveltimes of *P* and *PcP* waves. A clear intermediate arrival is visible throughout the network (pointed by arrows), and as distance increases, it comes closer to the first *P* arrival. At the top of Fig. 2(b), the source history of the earthquake is shown. It is obtained by aligning the actual first arrivals (applying dynamic station corrections) and summing them. Waves different from the direct *P* wave are expected to cancel out in the summation, considering the extension of the network (usually about 5°) along the great circle. The source history is fairly complex, but secondary arrivals at most stations (CDF, BSF, Hau, LDF, SSF, LPG2) cannot be attributed to this complexity, because of their strong amplitude. The coherency of the move out rules out source complexity and crustal reverberation as possible origins. The observations of the intermediate arrival is remarkably clear at the Vosgian stations CDF, BSF and HAU, where it is well separated from the first arrival. Finally, let us point out that the *PcP* wave is almost never visible in the data. A stack on the PREM theoretical *PcP* arrival (using static station corrections) does not display coherent *PcP* energy either. It

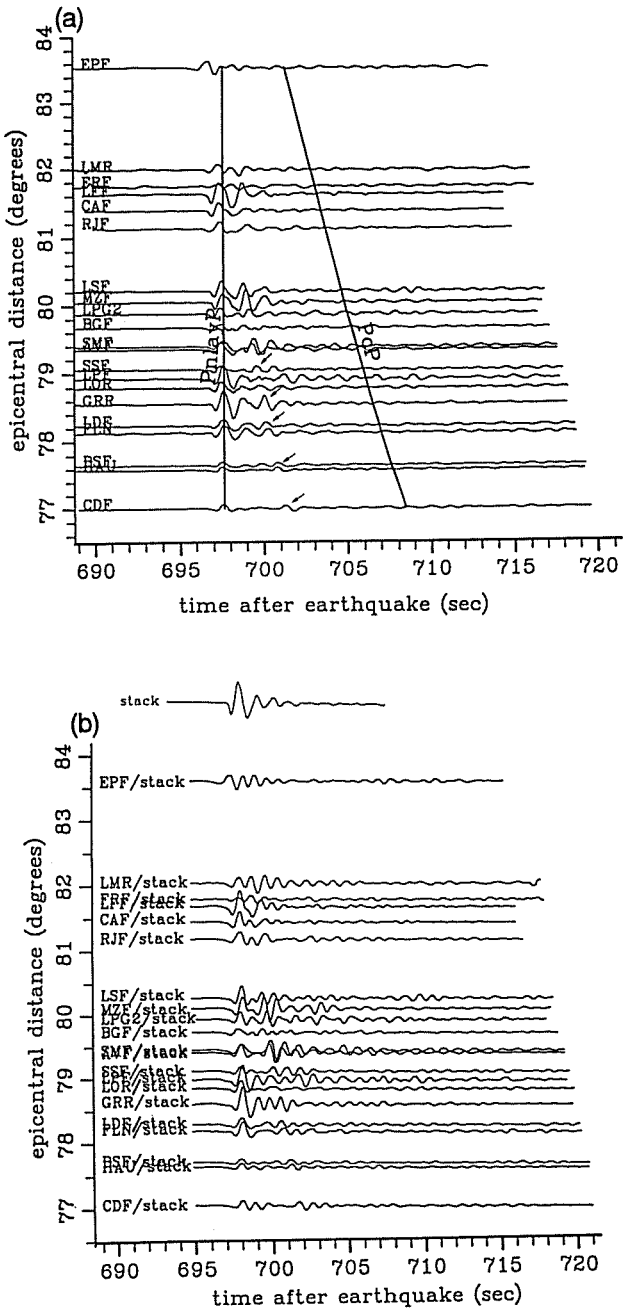

Figure 2. Seismograms for the Kamchatka earthquake of 1986 March 2. Both panels are *T*-Delta plots, for a selection of stations. Records are aligned on the theoretical *Pn*lay*P* arrival. The *Pn*lay*P* wave stands here for the direct *P* wave, travelling above a possible 'Lay discontinuity' at the top of the *D″* layer. The time scale applies to the station closest to the epicentre (the bottom one). (a) A Butterworth low-pass ($T > 0.3$ s) filter has been applied to the signals. The continuous lines are the theoretical traveltime curves for the *Pn*lay*P* and *PcP* waves. They set limits to the time window where anomalous waves that would originate in the lower mantle can be tracked. Clear secondary arrivals are visible throughout the network, and are indicated by arrows. (b) The same seismograms, deconvolved by the stacked seismogram (see text) of the 1986 March 2 event. The stack is displayed above, at the same time scale. Note the first peak for the *P* arrival. Secondary peaks are observed at the same stations as in Fig. 2(a), proving the validity of the deconvolution technique. A Butterworth band-pass ($T\epsilon[0.6–4]$ s) filter has been applied to the signals.

is not surprising given the very weak theoretical *PcP* amplitude in this distance range. For the same event, Weber (1993) observed both a *PdP* and a *PcP*, at the GRF narrow-aperture network.

Most often, anomalous arrivals can be detected at only a couple of stations, and hardly as clearly. Source complexities and crustal reverberations can thus indeed be responsible for some of the observations. In order to give a more objective assessment of these extra arrivals, the signals have been deconvolved from their corresponding earthquake source history.

This operation has already been described (Houard & Nataf 1992). A realistic source signal is obtained by stacking the L.D.G. seismograms aligned on the first *P*-wave arrival, using for each earthquake a set of dynamic station corrections.

For each of the 32 earthquakes (Table 1), a systematic search for anomalous arrivals situated between the theoretical *P* and *PcP* traveltimes has been conducted, using both deconvolved and raw signals (when the source duration was not too long). An example of this operation is shown in Fig. 2(b), again for the 1986 March 2 event. The stack used for the deconvolution is shown at the top of the figure. The deconvolved traces are plotted in the same way as in Fig. 2(a). Note that a clear peak marks the first arrival at most stations of Fig. 2(b), and secondary bumps are visible at many stations, like on the raw signals. Of sourse, since *PdP* arrivals are already particularly clear on the raw signals, Fig. 2(b) does not really illustrate the improvement that can be derived with this technique, but on the other hand, it demonstrates that the treatment is correct, since all *PdP* features are found again in the deconvolved traces.

For each earthquake, both relative T_{PdP}–T_P times and A_{PdP}/A_P amplitude measurements have been determined for each *PdP* wave between the *P* and *PcP* arrivals. About 200 anomalous arrivals have thus been found, on a total of more than 900 traces. For the Kuril events, most of them have been observed only at the Vosgian stations (BSF, CDF, HAU), closest to the epicentre, at distances comprised between 79° and 81°. See, for example, Fig. 2 of our previous paper (Houard & Nataf 1992), for the 1987 September 23 event. At these stations, the anomalous arrival is well separated from the first arrival. For stations at greater distances, clear well-separated secondary arrivals have rarely been observed. Filtering the data at high frequencies has sometimes been gainful (Houard & Nataf 1992). For the Kamchatka events, at shorter distances from the L.D.G network, many more observations have been obtained (see for example Fig. 2a). The most favourable distance range for these observations appears to be between 77° and 81°, or restrictively 78° to 80°.

RESIDUAL T_{PdP}–T_P TRAVELTIMES

In order to assess the origin of these extra arrivals, we have gathered the T_{PdP}–T_P measurements of all earthquakes together and plotted them versus the epicentral distance. The distances are initially corrected for focus depth (with a reference depth of 100 km). The correction amounts to 0.45° for each 100 km depth interval. It is the same for the PWDK (Weber & Davis 1990) and the PGLE (*P*-wave model 'copied' from the SGLE *S*-wave model of Gaherty & Lay

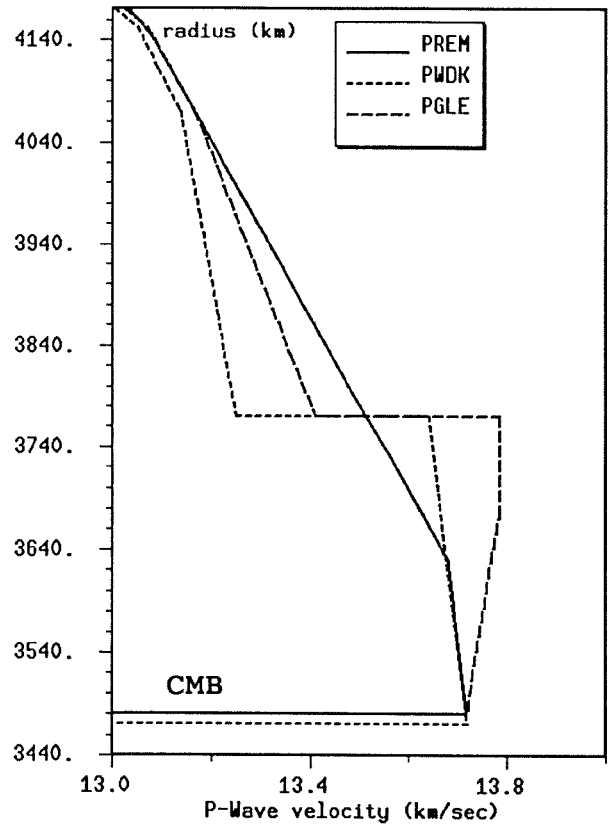

Figure 3. *P*-velocity distributions in the lowermost mantle. PREM is the Preliminary Reference Earth Model of Dziewonski & Anderson (1981). PWDK is the *P*-wave model of the lower mantle derived by Weber & Davis (1990). A 3 per cent *P*-velocity discontinuity is present at a radius of 3770 km. PGLE is the *S*-wave SGLE model of Gaherty & Lay (1992) transposed to *P* wave; it includes a 2.8 per cent discontinuity at the same radius. The respective curve symbols are shown in the insert, at the top right of the figure.

1992) models, whose velocity distributions are represented in Fig. 3 and compared to PREM (Dziewonski & Anderson 1981). The global $T_{PdP}-T_P$ data set (Fig. 4a) shows that the time residual roughly decreases as distance increases. However, a large scatter is present, especially due to 4 to 5 s residuals between 78° and 82°. This scatter is not really surprising. We are pointing at anomalous positive bumps on raw or deconvolved seigmograms. To be sure that the bumps are indeed connected to a deep mantle structure, the same bump should ideally be detected throughout the network, like in Fig. 2(a), at many different stations and different distances. But for most earthquakes, bumps are visible only at a few stations.

However, for seven of the 32 earthquakes (+symbol in the 'TENDENCY' column of Table 1), 10 to 15 anomalous arrivals have been found (on a total of 25 to 28 traces). Fig. 4(b) shows their corresponding residual time-versus-distance plot. The scatter is this time much smaller, with fewer residuals between 4 and 5s. This illustrates the importance of coherency in the pointing of the onsets. Also plotted are theoretical $T_{PdP}-T_P$ residual times for models PWDK (short dashes) and PGLE (long dashes). For synthetic signals, residuals have been measured in the same conditions as for

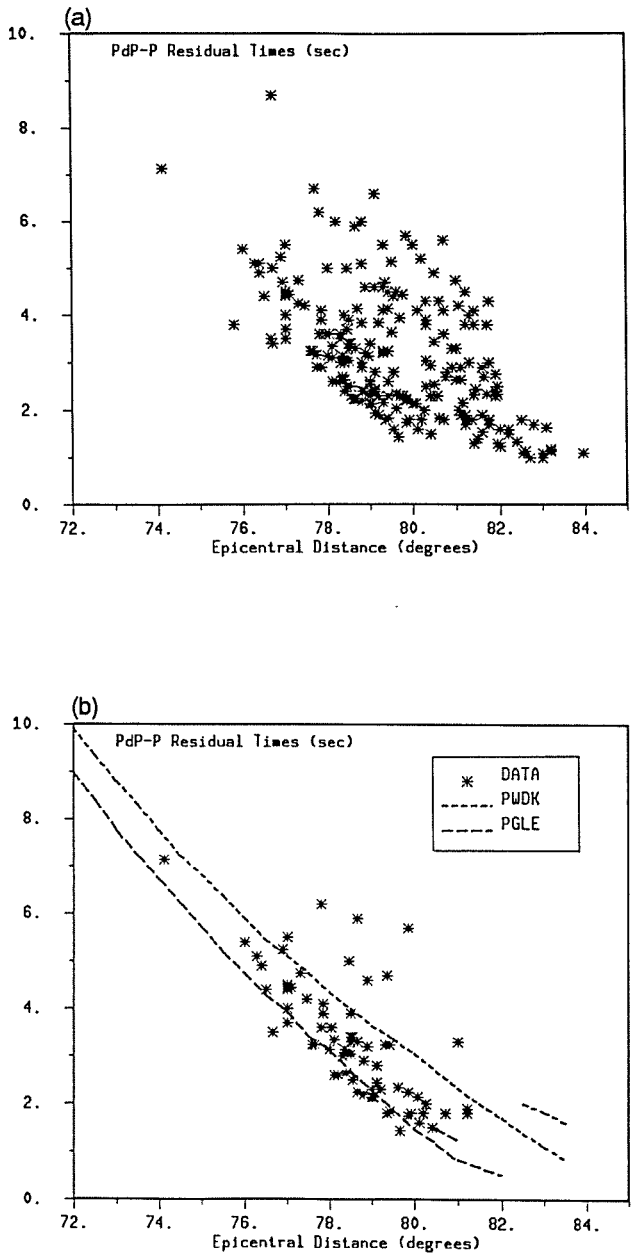

Figure 4. $T_{PdP}-T_p$ traveltime residuals. (a) Complete set of Kamchatka/Kuril events of Table 1. Note the rough decrease as distance increases, but also the greater scatter. 4 to 5 s residuals usually correspond to the observation of a supplementary anomalous arrival between *P* and *PcP*. The precision of the residuals' measurement is estimated to be 0.1 s. (b) 'Best' events of Table 1. For these events, at least 10 to 15 anomalous arrivals have been found, and the hand picking of the extra arrivals is expected to be more coherent than in Fig. 4(a). Theoretical $T_{PdP}-T_P$ curves for models PWDK and PGLE are also displayed. Theoretical residuals are measured in the same way as on deconvolved data (see text). Note that the scatter is smaller, and that the decreasing tendency of the residuals with distance is more obvious. The distribution of residuals is roughly comprised between the two theoretical curves.

deconvolved data: the impulse medium responses calculated with the WKBJ method have been low-pass filtered, and peak-to-peak measurements have been made. Note again that the residuals decrease as distance increases. They are

roughly comprised between those of models PGLE and PWDK, both displaying a *P*-velocity discontinuity 290 km above the core–mantle boundary.

ANOMALOUS WAVE ORIGINATING IN THE LOWER MANTLE

The scatter is still important in Fig. 4. Except for a few events, the coherency of the bumps we are pointing out is rather uncertain. In order to improve this coherency, we have decided to collect deconvolved signals from different earthquakes at **fixed stations** (one station alone, or couples of stations that are very close within the network). In this procedure, epicentral distances have been corrected from focus depth (see above in text). Moreover, **only traces for which a secondary arrival has been observed** have been kept. A total of 160 traces have thus been selected, for a total of 20 stations (stations with the greatest numbers of *PdP* observations). It is essential to collect **deconvolved** data in order to mix traces from different earthquakes. Figs 5(a) and (b) show deconvolved traces at stations AVF–SMF and BSF, respectively. For each trace, the name of the station is indicated, and the earthquake represented by a two-digit number (Table 1). The traces are all aligned on the first and major peak. All traces have the same maximum amplitude.

On Fig. 5(a), the anomalous onsets display a coherent tendency, as distance increases. A crustal reverberation just beneath AVF and SMF sites is thus ruled out. On Fig. 5(b), however, a secondary arrival about 4 s after the first peak can be observed (dots) on many traces. For the Vosgian BSF station, crustal reverberations could thus produce anomalous bumps in the signals, that can be mixed up with deep propagation effects. Nevertheless, other arrivals (arrows), with shorter residual times cannot be attributed to this near-receiver effect (see for instance BSF58, BSF65, BSF61, BSF60, BSF53).

The global conclusion for the 20 data sets altogether is that the hypothesis of crustal reverberations can be ruled out as a global explanation of these abnormal arrivals. However, care must be taken at some stations (eliminate 4 to 5 s residuals at BSF for example).

The most impressive illustration of these *PdP* arrivals is given in Fig. 5(c). A compilation of the most conclusive station-by-station record sections (AVF–SMF, CDF–HAU, SSF–LBF and LSF–TCF) has been made. It is perhaps the most complete *PdP*-wave record section ever shown, since the move out with distance can be followed clearly, with a good sampling, over more than 5°. This compilation of best recordings: (1) rules out the crustal reverberation hypothesis as a major explanation of *PdP* observations, (2) rules out any near-source-effect hypothesis, like diffraction by, or multipathing through, the Kuril subduction slab. The *PdP*-wave slowness is indeed about 0.8° less than that of the direct *P* wave. As extensively demonstrated by Weber & Davis (1990), if a ray with such a slowness is traced back from the receiver to the source region, where a diffraction or multipathing effect is expected, then a mislocation of several hundreds of kilometres occurs.

The only explanation compatible with: (1) direct *PdP* recordings (Fig. 2a), (2) residual $T_{PdP}-T_P$ measurements (Fig. 4), (3) station record sections (Fig. 5) 4) a $-0.8\,s°$ *PdP* residual slowness is a lower mantle origin. The *PdP* wave cannot but interact with a lower mantle reflector or discontinuity to satisfy all these observations.

At this point, it is interesting to underline the difference in the way Weber & Davis's (1990) or Weber's (1993) results and ours are derived. Weber & Davis' analysis is an event-by-event analysis. The GRF array is a local array, and if a stacking procedure is used, it can be considered as a single station with a very high signal-to-noise ratio. The detection of the *PdP* wave is thus possible even for very weak *PdP*/*P* amplitudes (for example at distances as short as 70°). The slowness-versus-time energy diagram (vespagram) technique helps to discriminate between a source complexity and a lower mantle anomaly. However, if a *PdP* wave is not detected at the GRF array, it may be hazardous to interpret it systematically as an absence of reflector at the top of *D″*. Dome-like lateral variations of the topography of the 'Lay discontinuity' can produce a local defocusing effect (Weber 1993), rending the *PdP* wave undetectable at GRF, but still observable further away. On the contrary, the *PdP* wave is rarely observable at all stations of the wider L.D.G network. Our observation of the *PdP* wave is more global. Except for exceptional events like the 1986 March 2 one (Table 1), our interpretation of the extra arrivals between the *P* and *PcP* waves as reflections in the lower mantle is mainly based on record sections where data from different earthquakes have been gathered up (Figs 5a and c). The data collection of Fig. 5c is built from records of 18 events. Whereas individual earthquake records do not support a clear interpretation (since the *PdP* wave is detected only at a few stations of the network), the *PdP* wave move out is particularly clear on global data sets (Figs 5a and c).

D″ STRUCTURE BENEATH NOVAYA ZEMLYA ISLAND

Investigating the *D″* structure

The extra arrivals between *P* and *PcP* have been clearly identified as reflections on a lower mantle discontinuity or reflector. As a first step, we will test if our observations can be accounted for by a unique mean spherical discontinuity structure, at the top of the *D″* layer. This 'Lay discontinuity' should produce a usual triplication feature. It is illustrated in Fig. 6, with WKBJ synthetics (Chapman 1976; Dey-Sarkar & Chapman 1978; Chapman & Orcutt 1985) calculated for the PWDK model (Fig. 3). The adequacy of the WKBJ method to model the L.D.G signals is explained in our previous paper (Houard & Nataf 1992). Compared to synthetics with model PREM (Fig. 3), it produces extra arrivals between *P* and *PcP*. The *Pn*lay*P*, *Pt*lay*P* and *Pr*lay*P* waves are respectively the direct *P* wave and the waves transmitted **through** and reflected **on** the 'Lay discontinuity'. Note that at distances before the theoretical cross-over, **where the *Pn*lay*P* wave is not affected by the discontinuity**, we will call the *Pn*lay*P* wave a *P* wave in text, for simplicity. Synthetic tests of various 'Lay' structures have revealed that the position of the triplication cross-over, and the synthetic waveforms beyond, were most sensitive to the *P*-wave velocity gradient above the discontinuity. For a same discontinuity depth, weak gradients, as in model PWDK, involve great cross-over distances and the existence

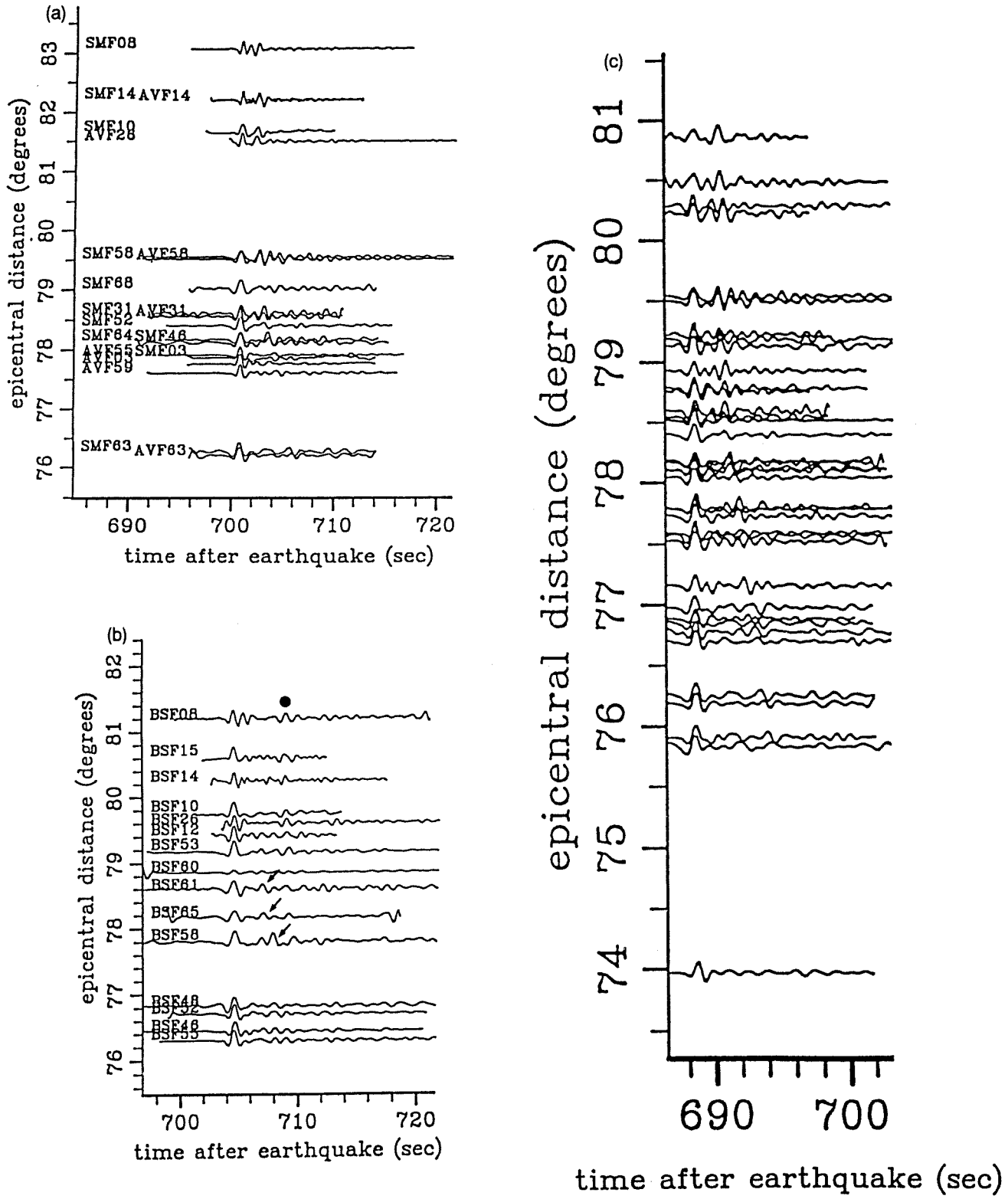

Figure 5. Record sections of deconvolved data **at given stations.** All traces are aligned on the first peak, and have the same maximum amplitude. For each earthquake, signals have been deconvolved by the corresponding stacked-source, bandpass filtered, and records of the same station (or couples of very close L.D.G stations) have been gathered. The numbers that follow the station name refer to earthquakes in Table 1. (a) Record section for the SMF and AVF stations, which are very close to each other (see Fig. 1). Note the clear move out of the secondary arrival, which comes closer to the first *P* wave as distance increases. (b) Record section for the Vosgian BSF station. Note the existence of a secondary arrival (black dot), at a constant traveltime residual of about 4.5 s (BSF65, BSF61, BSF53, BSF12, BSF26, BSF10, BSF14, BSF08). It indicates that reflectors just beneath the station may be responsible for it. Note also the existence of a set of other anomalous arrivals (arrows), at shorter arrival times (BSF58, BSF65, BSF61, BSF60, BSF53). As in Fig. 5(a), they come closer to the first *P* wave as distance increases. Finally, interferences between these two anomalous arrivals may be observed at the shortest distances (BSF55, BSF46). (c) Selection of the 'best' record sections of deconvolved data grouped station by station. Again, note the clear move out of the secondary arrival as distances increases. It can be followed on more than 5° of epicentral distance, with a good density of observations.

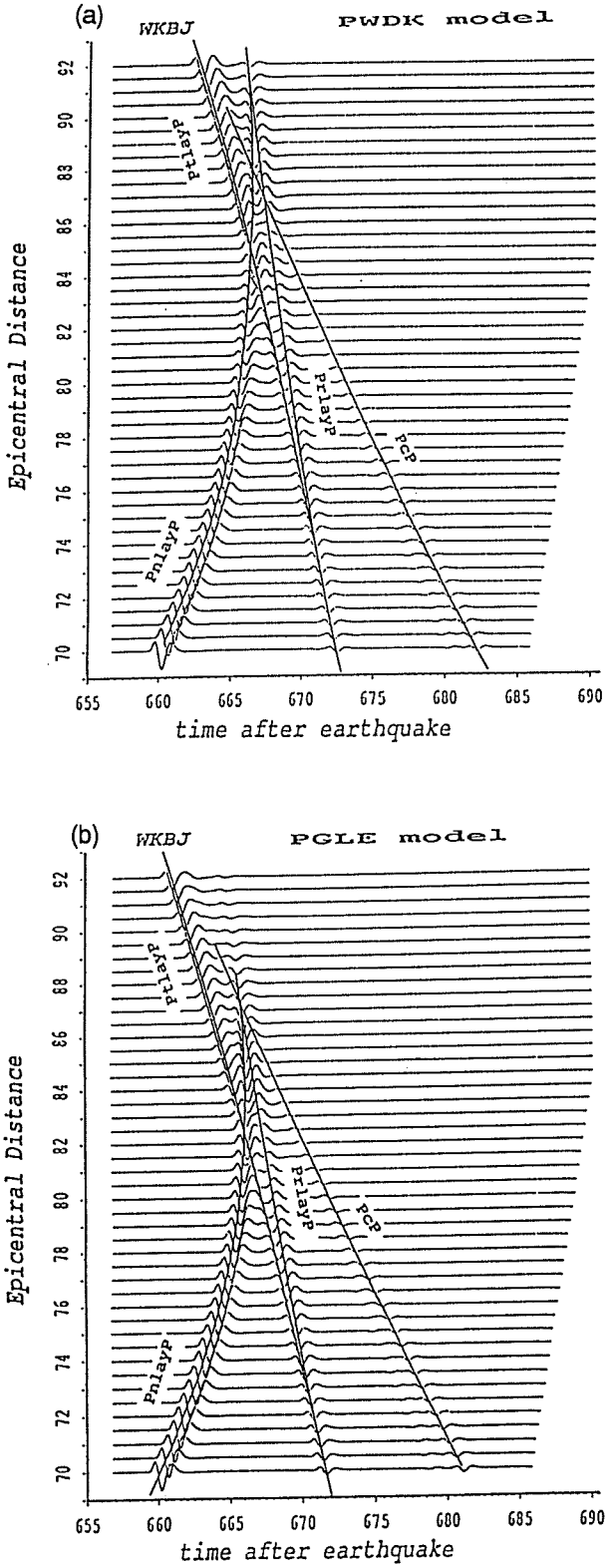

Figure 6. Synthetic seismograms computed with the WKBJ method, between 70° and 92°. Times are reduced using a 5.2 s/° slowness, and times at the bottom apply to the station at 70°. Continuous curves are the theoretical traveltime curves for the *Pn*lay*P*, *Pt*lay*P*, *Pr*lay*P* and *PcP* waves. The focus depth is 100 km. The impulse responses have been convolved with a causal t^* attenuation operator (Chapman *et al.* 1988), and with the L.D.G instrument response. Note the existence of a secondary arrival between the *Pn*lay*P* and *PcP* waves, and the waveform complexities around the triplication cross-over. The theoretical amplitude of the *PcP* wave is found very weak at this epicentral distance range. Note that because the analytical impulse response is convolved in the algorithm, by a 2**dt* boxcar filter (where *dt* is the time sampling rate), WKBJ traveltime curves do not match the first onsets (Chapman *et al.* 1988). (a) Seismograms calculated for the PWDK model (Weber & Davis 1990). The cross-over distance is about 85°. (b) Seismograms calculated for the PGLE model (copied from the SGLE model of Gaherty & Lay 1992). The triplication cross-over occurs at about 83°. Unlike in Fig. 6(a), the second *Pn*lay*P* + *Pr*lay*P* branch is quite weak around 90°.

of two arrivals at distances as far as 90° (Fig. 6a); in comparison, larger gradients, as in model PGLE (Fig. 3), produce shorter cross-over distances, and only one arrival is clearly visible at 90° (the *Pn*lay*P* + *Pr*lay*P* diffraction occurs at a shorter distance), as can be seen in Fig. 6(b). Another consequence is of course that $T_{PdP}-T_P$ residuals (*PdP* stands here for *Pt*lay*P* + *Pr*lay*P*) are smaller for model PGLE than for model PWDK.

Investigation of the *D″* structure beneath the Novaya Zemlya Island can thus be conducted in several directions: (1) use the traveltime residuals to infer the depth of the discontinuity and the velocity gradient above it, (2) use supplementary data, at epicentral distances between 88° and 90° to set limits on this gradient, (3) use the first arrival traveltimes as an additional constraint.

Though the move out of the *PdP* wave is well observed between 74° and 79°, with a −0.8 s° residual slowness, it is no longer clear beyond 79°. As can be seen on Fig. 5(c), the secondary arrival seems to get parallel to the first arrival, whereas one would expect it to cross it, as a continuation of the 74°-79° distance range trend. The reason may be that most of the deconvolved traces of Fig. 5(c) beyond 79° correspond to earthquakes with larger $T_{PdP}-T_P$ residuals ('INTERMEDIATE' tendency) than in the 74°–79° range ('LAY' tendency). However, it is a general observation that if *PdP* observations are rather clear at short distances, where the *PdP* is separated from the direct *P* wave, clear evidence of a *P*/*PdP* interaction at larger distances is rarely observed (even in the 860302 event of Fig. 2). We tried thus to test possible waveform complexities within the data in the distance range where the *P* and *PdP* waves should come together. Comparisons between data and synthetics have been made. The synthetics were calculated for radial structures of *D″*, and the impulse responses convolved with the stacked 'source' of the earthquake. This procedure gave rather poor results. It has not been possible to test the existence of a *PdP* contribution, between 82° and 88°, in the data waveforms. A 1-D approach is obviously too simple, as well as the use of single traces for the data.

Traveltime residuals

Traveltime residuals have been widely used to infer regional *D″* structures. Weber & Davis (1990) have used $T_{PdP}-T_P$ residuals, whereas Gaherty & Lay (1992) preferred $T_{ScS}-T_S$ and $T_{ScS}-T_{Scd}$ residuals (Scd is the equivalent for *S* waves of the *PdP* wave). Inferring the structure of the 'Lay discontinuity' requires a relatively coherent residual-time

data set. This is obviously not the case on Fig. 4(a), where all 200 observations have been represented. Fig. 4(b) looks better, but too few points are present. The question is: why is the scatter so great in Fig. 4a? It seems doubtful that it should be thouroughly accounted for by lateral variations of the depth of the discontinuity. Maybe the residual time distribution is contaminated. A more coherent data set could thus be extracted once the contamination has been eliminated. As mentioned previously in text, crustal reverberations can produce positive onsets on raw or deconvolved signals that are not correlated to deep propagation in the mantle. It is the case at station BSF, for 4 to 5 s residuals, and those must be eliminated. Another source of contamination may result from propagation effects in the source region, through the Kuril subducted slab. Depending on the geometry of the slab and on the depth of the earthquake, the propagation of the *P* and the *PdP* through the slab (with different dip angles) can alter $T_{PdP}-T_P$ traveltime residuals by up to 1.5 s (Weber & Davis 1990; Weber 1990). A third source of contamination may occur if the deconvolution from the source history of the earthquake is of bad quality, especially if the source is complex. The variability of the first *P*-wave motion throughout the network, emergent *P* waves and small errors in the hand picking of the first arrival may rend our stack somewhat biased. Automatic multichannel cross-correlation techniques (Vandecar & Crosson 1990) could surely improve the quality of the stack. Let us point out that residuals of Fig. 4(a) have been measured both on raw and deconvolved signals, and that only coherent measurements have been kept. However, in the case of a rather long source duration, with multiple wavelets, observations on raw signals have been discarded, and measurements have been made on deconvolved data only. The precision in the hand picking of the residuals can be estimated to 0.1 s.

To check whether contamination of either type is present in the distribution of Fig. 4(a), we have plotted the residuals **earthquake by earthquake,** along with the theoretical curves for models PWDK and PGLE. This procedure has lead to two important results: (1) on the 30 earthquakes that contribute to Fig. 4(a), the residual times of 12 of them have been rejected. As a matter of fact, either they displayed a constant value whatever the distance was (maybe due to the inaccuracy of our stack), or dispersion was found too large for them to be trusted. The 12 earthquakes are easily identified by a 'NONE' item in the 'TENDENCY' column of Table 1. (2) Two different residual time versus distance tendencies have emerged for the remaining events. A first group of eight events, all from the Kamchatka region, and including the 1986 March 2 event of Fig. 2(a), display rather small residuals that roughly align on the PGLE theoretical curve. They are identified by a 'Lay' item in the 'TENDENCY' column of Table 1. A second group of 10 events, four in Kamchatka and six in the Sea of Okhotsk, follow a tendency which is intermediate between those of models PWDK and PGLE. They are identified by an 'INTERMEDIATE' item in the 'TENDENCY' column of Table 1. The residuals of these 18 events are displayed versus distance in Fig. 7, along with the theoretical PWDK and PGLE curves. 4 to 5 s residuals at the BSF station have also been eliminated. Compared with Fig. 4(a), the dispersion is smaller, and the two previous tendencies

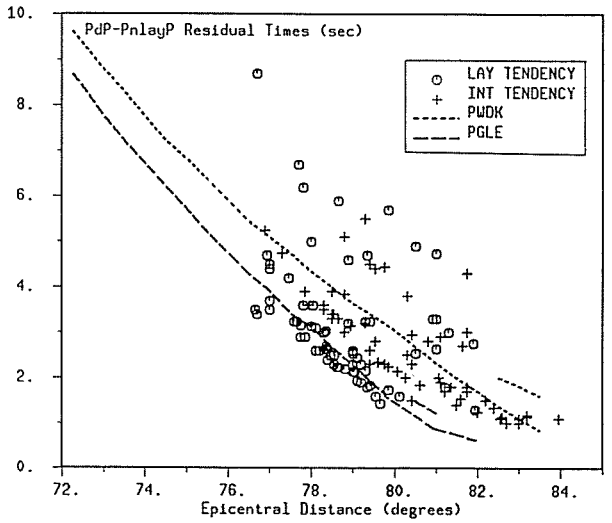

Figure 7. $T_{PdP}-T_P$ traveltime residuals for the Kamchatka/Kuril events of Table 1. Only events with a clear traveltime residual versus distance trend (see text) have been selected (see Table 1). Theoretical $T_{PdP}-T_P$ curves for models PWDK and PGLE are also displayed. The symbols of the drawings are shown in the insert, at the top right of the figure. The cross-symbol tendency is intermediate between the two theoretical curves, whereas the circle-symbol tendency is close to that of the PGLE model. For each tendency, the scatter of the residual-times distribution is smaller than that in Figs 4(a) and (b).

emerge clearly. Cross symbols represent the 'INTERMEDIATE' tendency, whereas circles stand for the 'LAY' tendency.

Before deriving *D″* radial models, a crucial question is whether the two residual tendencies have a geographical coherency or not. *Prlay*P bounce points have been calculated for all epicentre-station couples (the focus depth is taken into account). Fig. 8 is an equal-area projection of these bounce points. Symbols refer to the corresponding residual tendencies. Note that circles are all grouped north of Novaya Zemlya Island, and correspond to events located in the southern tip of Kamchatka. Crosses are present in two different disconnected regions: southeast and northwest of the Novaya Zemlya Island. The first region corresponds to all Kuril/Sea of Okhotsk events of our list (Table 1). The second is for Kamchatka events, but which location is northeast of the Kamchatka southern tip corresponding to circle symbols. The existence of a geographical coherency is quite clear, and hence the existence of regional lateral variations in the *D″* structure beneath Novaya Zemlya Island. The pattern of the lateral variations appears to be complex, since the circle symbol region is embedded within two cross symbol regions. The scale of the lateral variations can be compared with the theoretical Fresnel zone of the data, displayed in the top part of the figure. Weber & Davis (1990) have sampled *D″* not far away, southeast of Novaya Zemlya Island (Fig. 11 in their paper). Triangle symbols are also represented, south of the previous regions. The bounce points refer to earthquakes located in Japan or the Ryukyu Islands. They provide larger epicentral distances and will contribute to the next section of the paper.

Since we showed that lateral variations exist in the *D″* structure beneath Novaya Zemlya Island, deriving a unique

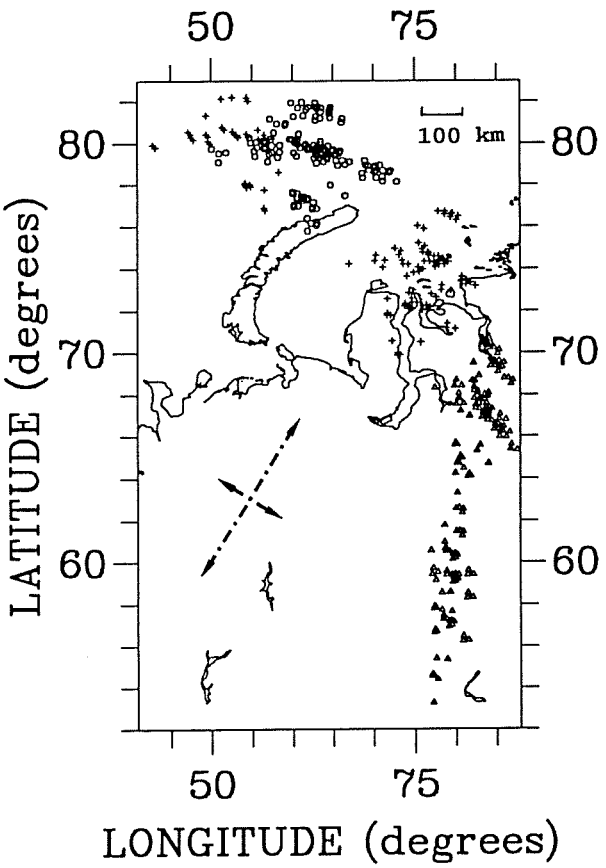

Figure 8. Map of the bounce points of the *Pr*lay*P* wave at the top of *D″*. Kamchatka/Kuril events with a T_{PdP}–T_P 'LAY' tendency (see Table 1) are represented by circles, and those with an 'INTERMEDIATE' tendency by crosses. Note that the two different symbols cover different geographical regions. 'INTERMEDIATE' and 'LAY' tendency symbols are only representative of global features. They do not map the detectability of the *PdP*-wave event by event and station by station. The scale of variation from one tendency to the other can be compared with the theoretical T/4 Fresnel zone, whose axes are represented by dashes in the bottom left part of the figure. Note that one latudinal degree represents here 50 km at the top of *D″*. The triangles represent the bounce points of the *Pr*lay*P* wave for the Honshu/Ryukyu Islands earthquakes of Table 2. In this case, the *Pr*lay*P*-wave bounce point and the *Pt*lay*P*-wave turning point are significantly distant from each other. The triangles thus give only a global indication of the *D″* area sampled by the waves.

radial velocity model becomes vain. Deriving two *D″* structures (one for each tendency) remains somewhat limited, but it allows us to set limits both on the depth of the discontinuity and on the gradient above it. Anyway, the derivation of 1-D structures seems rather realistic given the large coverage of our *PdP* observations (Fig. 5c). The procedure used to derive models is explained in the Appendix. The scattering of the two residual time distributions of Fig. 7 (circle and cross symbols) creates some unprecision in the 1-D structures derived. Thus, for each tendency, extreme radial structures that match the residuals are displayed in Figs 9(a) and (b). For both tendencies, velocity gradients above the discontinuity are found larger than in the PWDK model, and smaller than in PREM. For the cross symbol tendency (Fig. 9a), the radius of the discontinuity ranges from 3730 to 3770 km. The *P*-velocity jump at the discontinuity is of about 2 per cent. However, relative A_{PdP}/A_P amplitudes are highly variable from one earthquake to another and the radial models derived only roughly satisfy the amplitude ratio distribution.

For the circle symbol tendency (Fig. 9b), the radius of the discontinuity ranges from 3740 to 3780 km. The *P*-velocity jump at the discontinuity is again of 2 per cent, but the circle symbol tendency requires a larger upper velocity gradient than the cross-symbol tendency.

Since the *PcP* wave is never detected on the L.D.G network in the 75°–82° distance range (even for the very nice 1986 March 2 event), we have no precise constraint on the gradient below the 'Lay discontinuity'. As a consequence, a trade-off exists between the depth of the discontinuity and the *P*-velocity jump at the discontinuity, **but only to a certain extent.** Indeed, a high *P*-velocity jump can produce drastic changes in the synthetic waveforms and amplitudes, especially if the gradient above the discontinuity is large. At short distances, the *Pt*lay*P* and *Pr*lay*P* waves are very close to each other and produce only one secondary peak. But as distance increases, the *Pt*lay*P* wave, which travels through the 'Lay discontinuity', arrives earlier than the *Pr*lay*P* wave and their separation produces two secondary arrivals. The distance at which the separation occurs depends of course on the depth of the discontinuity and on the gradient above it (compare for example Figs 6a and b), **but also on the velocity jump at the discontinuity.** High-velocity jumps produce a splitting at shorter distances. The destructive interference between the *Pr*lay*P* and *Pt*lay*P* waves give then very low $A_{Pt\text{lay}P}/A_P$ and $A_{Pr\text{lay}P}/A_P$ amplitude ratios. Though our constraint on the velocity jump at the discontinuity is rather poor (see above in text), our preferred structures of *D″* (Figs 9a and b) are not compatible with *P*-velocity jumps higher than 3 per cent.

Observations beyond the theoretical cross-over

As mentioned previously, the region with coherent *PdP* observations is rather large (Fig. 5c). For this reason, deriving 1-D structures of *D″* may not be so unrealistic. **In the hypothesis that such 1-D structures may extend further south in northern Siberia** (triangle symbols of Fig. 8), it may be interesting, as a second step, to investigate the *D″* structure at distances well beyond the theoretical cross-over (85° for model PWDK, Fig. 6a). Of course, this hypothesis may be wrong: whereas Gaherty & Lay (1992) have sampled the same *D″* region (Fig. 2 in their paper), in the 75–85° range, with *S* waves, and reported extra arrivals between *S* and *ScS* waves (interpreted as waves reflected on a discontinuity 290 km above the core–mantle boundary), Weber (1993) finds no anomaly for *P* waves in the same area.

Accurate signals in the 88–92 distance range from the L.D.G network are provided by Honshu and Ryukyu Islands earthquakes. 10 earthquakes have been selected, using the same criteria as those mentioned in the Data Section. They are listed in Table 2. Unfortunately, they do not display impulsive source histories, and *P*-waves first motions are often emergent. Once more, the deconvolution technique has appeared essential to obtain more objective observations of possible anomalous waves. On a total of 200

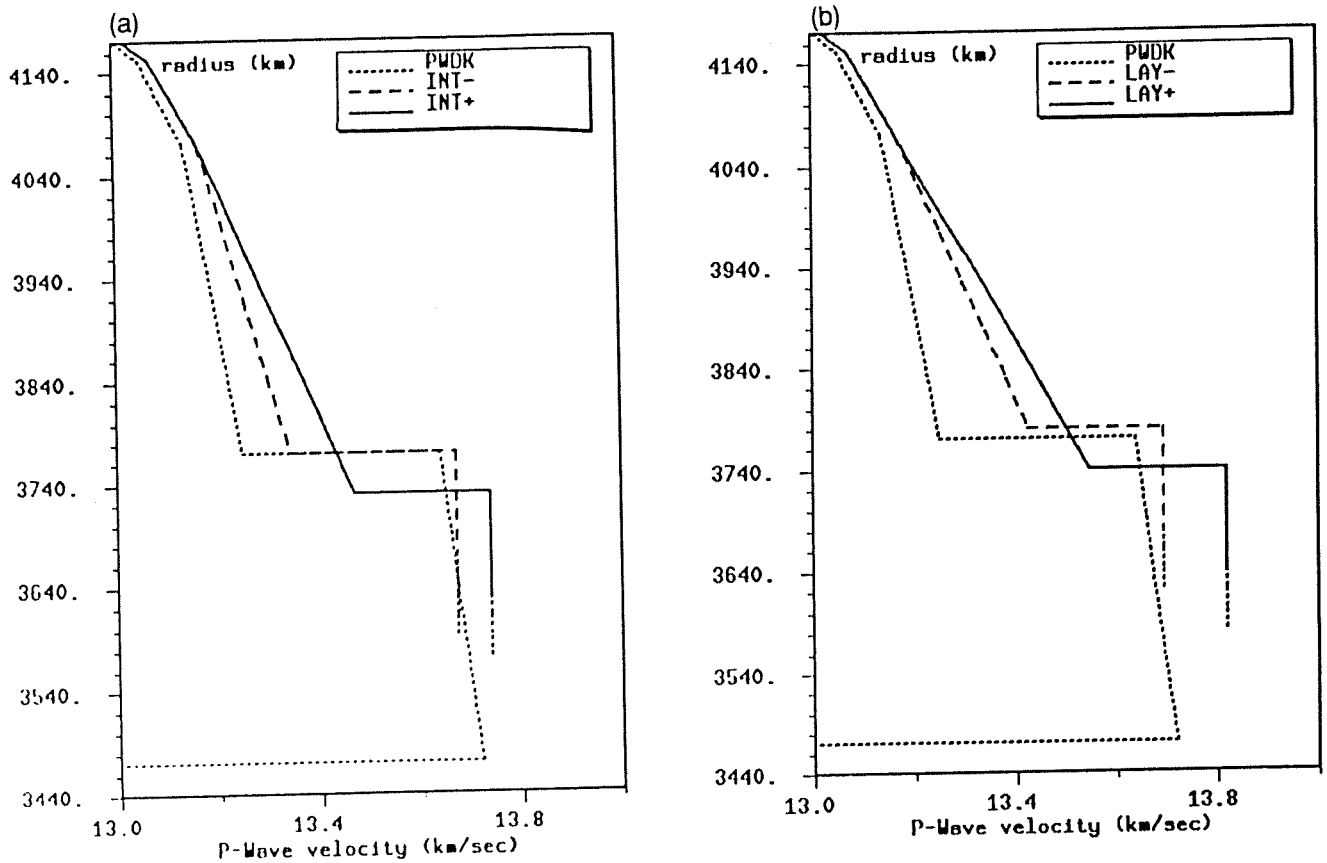

Figure 9. *P* velocity distributions in the *D″* layer. The PWDK model of Weber & Davis (1990) is compared with *P*-velocity structures that match the $T_{PdP}-T_P$ residual time distributions of Fig. 7. (a) Extreme velocity distributions that match the 'INTERMEDIATE' tendency of Fig. 7. INT – has the lowest gradient above the discontinuity, and INT+ the highest. The models are prolongated by dashes up to 100 km below the discontinuities, since the 75°–82° distance range (for which residuals are measured) is too short for waves to sample the lowermost part of the mantle (the *PcP* wave does, but was never detected on the network). (b) Same as a for the 'LAY' $T_{PdP}-T_P$ residual-time tendency.

deconvolved traces, 55 clear anomalous onsets have been found within 10 s after the first peak. A selection of these traces is displayed in the $T-\Delta$ plot of Fig. 10(a). All traces have the same maximum amplitude. No coherent secondary arrival is observed as distance increases, unlike in Figs 2(a), 5(a) and 5(c), in the 75–85° epicentral distance range. Theoretical WKBJ impulse responses are given (Fig. 10b) in the same distance range, calculated for the PGLE model (Fig. 3), for comparison. On both panels of Fig. 10, seismograms are aligned on the first arrival. Bounce points

Table 2. Honshu/Ryukyu Islands seismic region.

n°	date (y/m/d)	time (h:mn:s)	lat (deg)	long (deg)	depth (km)	mb	$TS_{1/2}$* (sec)	region	Source
69	83/06/21	17:06:51.5	29.7	129.4	159.	5.8	3.4	Ryukyu Is	ISC
70	83/11/16	10:44:07.8	37.4	141.5	53.	5.5	1.7	Honshu	ISC
71	85/07/28	19:33:21.9	37.4	140.5	95.	5.3	1.7	Honshu	ISC
72	85/10/04	12:25:51.7	35.8	140.1	83.	5.7	3.4	Honshu	ISC
73	86/06/24	18:45:30.8	34.9	140.7	60.	5.4		Honshu	ISC
74	86/10/13	21:17:50.6	37.1	141.0	63.	5.8	2.4	Honshu	ISC
75	86/11/28	22:29:36.6	36.4	141.1	52.	5.6	3.1	Honshu	ISC
76	87/07/03	10:10:43.7	31.2	130.3	167.	5.6	3.0	Ryukyu Is	ISC
77	89/03/17	02:21:55.5	27.1	127.4	91.	5.7	2.7	Ryukyu Is	ISC
78	90/05/03	07:43:45.0	36.4	140.5	64.	5.4	1.6	Honshu	USGS

Earthquakes' parameters are from ISC or USGS bulletins.
*: Source half-durations are from preliminary determination of epicentres (P.D.E) bulletins.

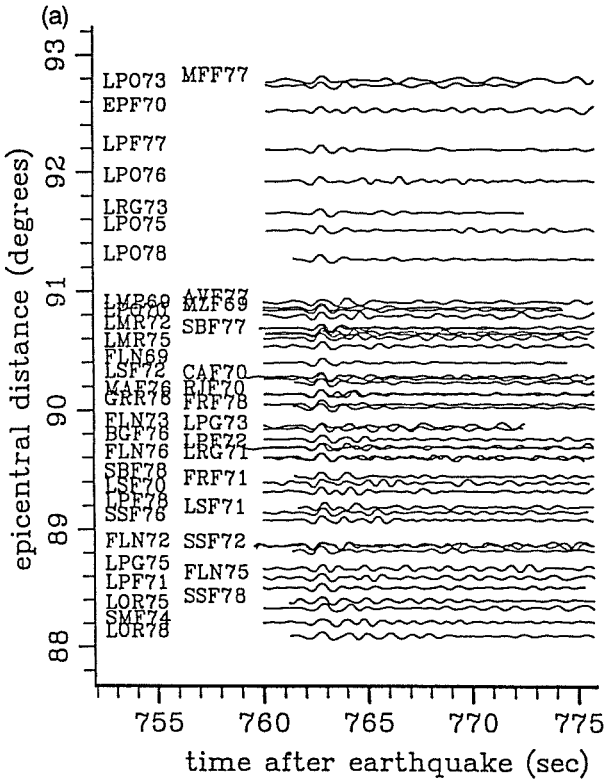

Figure 10. (a) Deconvolved signals for the Honshu/Ryukyu Islands earthquakes of Table 2. Only traces for which secondary arrivals have been found are shown. The set-up is the same as in Fig. 5. Unlike in Fig. 5, no arrival with a coherent move out with distance is visible. (b) WKBJ impulse response synthetics are shown, in comparison, in the same distance range, as calculated for the PGLE model. Note the existence of a second *P* branch with a large amplitude near 88°. It is diffracted on the 'Lay discontinuity' and decreases rapidly beyond 90°. It is not observed in the data.

of the *Pr*lay*P*-wave travelling from the Honshu–Ryukyu Islands region to the L.D.G network are plotted in Fig. 8 (triangle symbols).

As formely discussed, radial models of *D″* with low gradients above the discontinuity would imply the existence of two distinct *P* branches between 88° and 92° (PWDK model, Fig. 6a), whereas large gradients would produce only one branch (PGLE model, Figs 6b and 10b). Depending on the gradient value, the *Pn*lay*P* + *Pr*lay*P*-wave diffraction on the 'Lay' discontinuity happens at shorter or larger distances, and hence the amplitude decay within the shadow zone.

If the *P*-wave anomaly extends further south in northern Siberia (which was the basic assumption of this section), our analysis in the 88°–92° supports the existence of rather high gradients above the discontinuity. Note that observations of Gaherty & Lay (1992) and Weber (1993) and ours are not contradictory since the same *D″* zone is not sampled at the same epicentral distances. **If our basic assumption can be ruled out,** our observations just confirm the absence or the undetectability of a discontinuity in this area.

Note that WKBJ amplitudes for diffracted waves in the far shadow are over-estimated (Richards 1976). The correct amplitude decay within the 'Lay' discontinuity shadow would be somewhat stronger, as predicted by a reflectivity

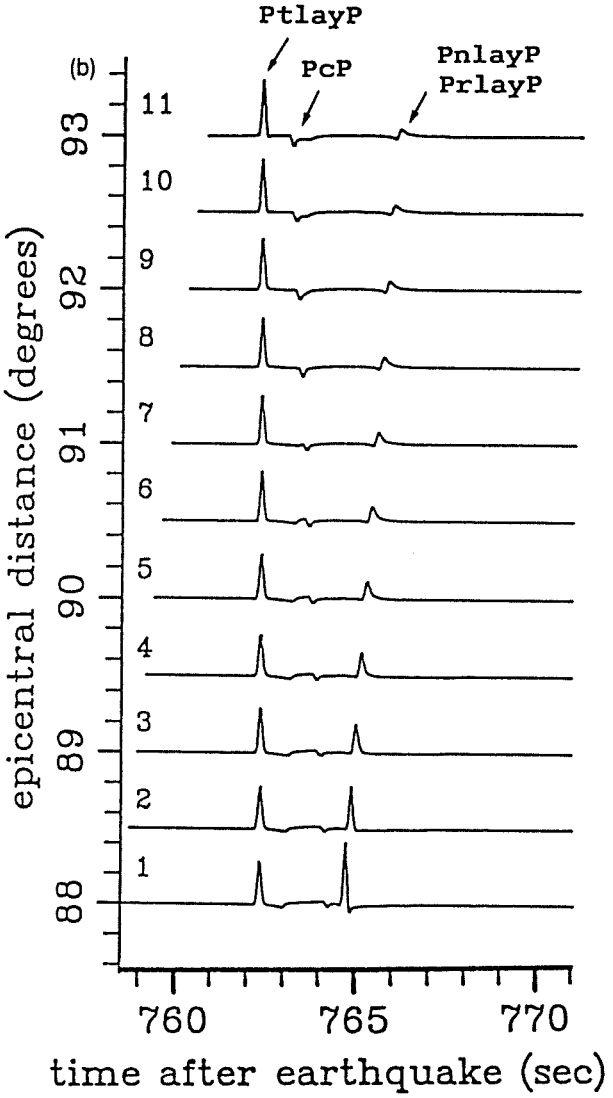

Figure 10. (*Continued*).

algorithm (Chapman & Orcutt 1985). Note also that the existence of topography on the 'Lay' discontinuity could reduce the detectability of the second branch beyond the triplication cross-over (Thorne Lay, 1992 personal communication), as often observed for upper mantle triplications. The reason is that waves grazing an interface are very sensitive to small topography variations.

Hodochrones of the first *P* arrival

To obtain a 'Lay discontinuity' model, the PREM reference velocity distribution is perturbed below a radius of 4070 km. The gradient just above the discontinuity itself can thus be very different from that in PREM (Fig. 3). Its value is essential for the theoretical $T_{PdP}-T_P$ residual times to match the data. However, if direct *P* waves do not travel below 4070 km for distances shorter than 70°, it is no longer the case in the 80°–90° distance range, where they become more and more grazing on the discontinuity. Their theoretical traveltimes should then be greatly affected by the gradient value.

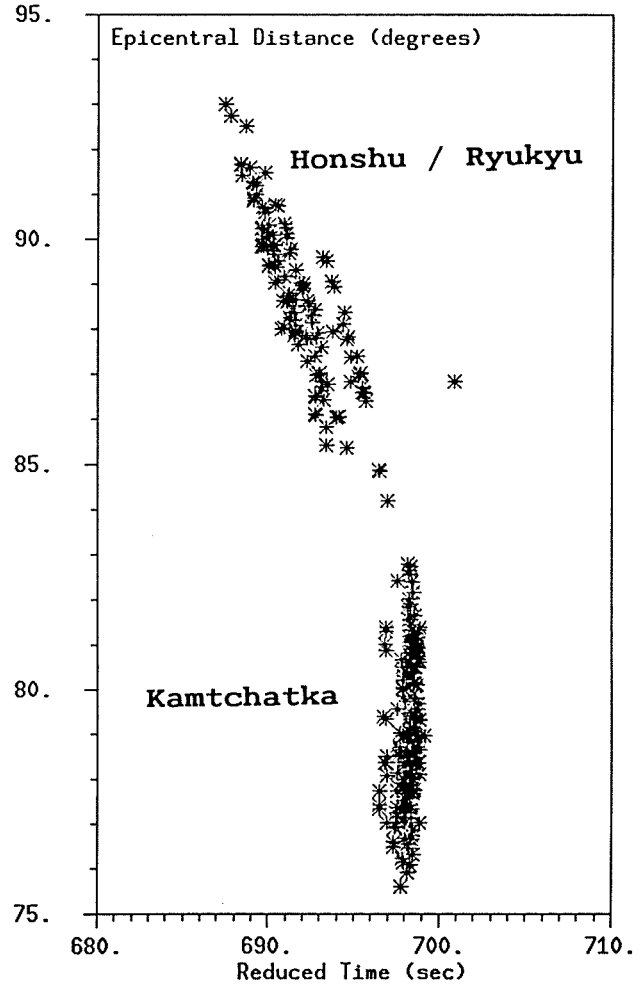

Figure 11. Hodochrones of the first *P* arrival. For a reference focus depth of 55 km, first *P*-wave onsets have been picked and static station corrections have been applied (see Appendix of Houard & Nataf 1992). Points with an epicentral distance less than 83° correspond to earthquakes of the Kamchatka seismic region, and those beyond 85° to the Honshu/Ryukyu Islands region. Times have been reduced with a 5.5 s/° slowness. Note the significant slowness decrease between the 75°–83° and the 85°–93° distance ranges. Unfortunately, for this focus depth, the data do not sample the intermediate 83°–85° distance range.

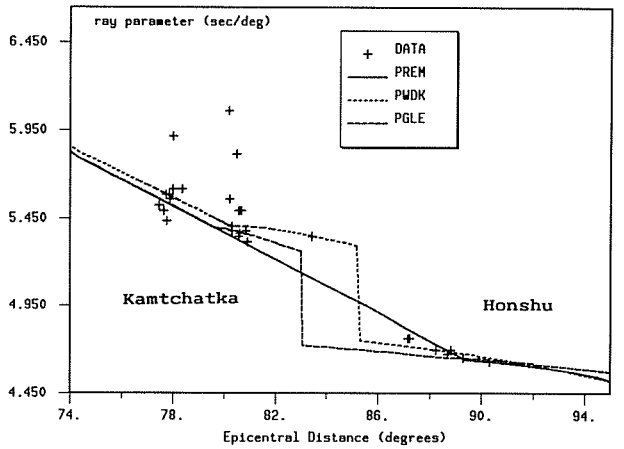

Figure 12. *p*-Delta plot for the reference focus depth of 55 km. The data slownesses have been obtained for each earthquake using a linear regression procedure, and the result has been attributed to the centre of mass of the epicentral distances. The slowness decrease observed in Fig. 12, between the 75°–83° and 85°–93° distance ranges, is retrieved. Theoretical *p*-Delta curves are also displayed for the PREM, PWDK and PGLE models. Note that all three models match the data well.

It is thus interesting to determine which discontinuity models are compatible with the first *P*-wave traveltimes. To construct the hodochrones, we have first gathered earthquakes with very similar focus depth. Four different reference depths have been selected: 55, 98, 130 and 575 km. For each group, first *P*-wave onsets have been picked and collected, *and static station corrections have been applied* (as described in the Appendix of Houard & Nataf 1992). The most important collection is obtained for the 55 km depth. More than 300 points are drawn in Fig. 11, in a reduced-time $T-\Delta$ plot. All points with epicentral distance **less than 83° correspond to earthquakes of the Kamtchatka region,** and points **beyond 85° to earthquakes in the Honshu–Ryukyu Islands seismic region.** Times have been reduced with a 5.5 s° slowness. A significant slowness decrease is observed between the 75°–83° and the 85°–93° distance ranges. Global traveltime shifts are visible in the 85–93° branch, but the three alignments are parallel. Unfortunately, because of the data selection, the 83°–85° range is not sampled. It would have helped determining whether the two branches connect smoothly, as in the absence of discontinuity, or abruptly (Figs 6a and b) as at a triplication cross-over, where the *Pt*lay*P* wave arrives earlier than the direct *Pn*lay*P* wave.

The corresponding $p-\Delta$ graph is shown in Fig. 12, along with the theoretical curves. Theoretical $p-\Delta$ propagation tables are directly provided by the WKBJ algorithm (Chapman, Chu & Lyness 1988). For the data, slownesses have been obtained for each earthquake separately, so that the global shifts of Fig. 11 are eliminated. A linear regression procedure has been carried out on 1° to 2° segments, and *p* values attributed to the centre of mass of the epicentral distances. PREM (or iasp91), PWDK and PGLE models match the data well. The 0.8 s/° slowness decrease between 80° and 88° is well reproduced.

The three other $p-D$ data sets are smaller. Fig. 13 shows the results for the 98 km reference depth, for which the theoretical 82°–85° cross-over distance range is sampled. The data display a rather smooth decreasing pattern. PWDK and PGLE theoretical curves do not match the data well. As a matter of fact, the existence of a 'Lay discontinuity' produces a 0.8 s/° slowness jump in the $p-D$ curves. For the PGLE model, the *Pt*lay*P* branch contributes to the $p-D$ curve beyond 83°, and slownesses are thus too small in the 83°–85° distance range to match the data. For the PWDK model, the cross-over occurs at about 85° (at this focus depth). The *Pn*lay*P* branch contributes at distances shorter than 85° producing slownesses that are too large, whereas the *Pt*lay*P* branch contribution beyond 85° and 87° is found too small. Actually, whatever the cross-over distance (and thus whatever the discontinuity model) is, the slowness jump involved is too large to match the smooth pattern of the data.

However, it has appeared necessary to compute the

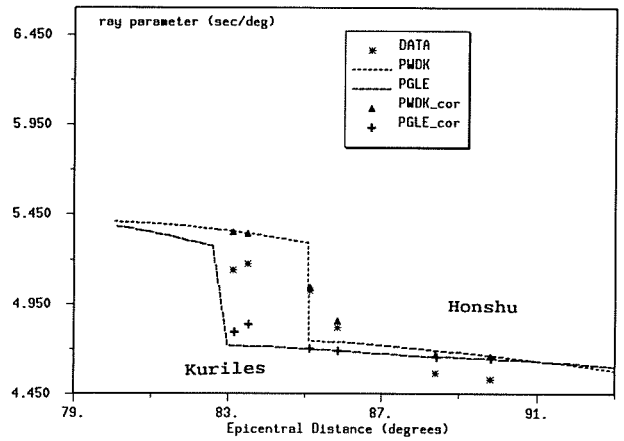

Figure 13. Same as Fig. 13 for the 98 km reference focus depth. Theoretical p-Delta points are also calculated with the linear regression procedure used for the data. Note the effect of the procedure for the PWDK model. Points near the PWDK triplication cross-over distance are shifted to intermediate positions, smoothing the original theoretical PWDK pattern.

theoretical p–Δ curves in the same way as the corresponding data, namely with a segment-by-segment linear regression technique. The reason is that when the same distance interval used for the data samples on both sides of a D'' model triplication cross-over, the p value derived with the regression involves contributions from both Pnlay$P$ and Ptlay$P$ branches. The p value at the centre of mass is thus bound to be significantly different from the value derived directly from the WKBJ propagation tables. The theoretical p–Δ curves of models PWDK and PGLE (Fig. 3) have thus been recalculated for all four reference depths.

For the 55 km data set, only one point (for the PGLE model) was well off the theoretical continuous-line curves and the conclusion is unchanged. For the 98 km data set, the new treatment has produced significant changes for the PWDK model. Around 84°, its new theoretical points (triangle symbols) have p values intermediate between those of branches Pnlay$P$ and Ptlay$P$, and are much closer to the data than the corresponding theoretical continuous curve. However, For the PGLE model (cross symbols), nothing is changed, since the cross-over distance is shorter. For the 130 km data set, the opposite phenomenon occurs, because some distance intervals in the linear regression procedure sample the PGLE model triplication cross-over distance range.

The determination of slownesses using a linear regression technique is a smoothing procedure, and abrupt changes in the first arrival slowness (as expected with D'' models with a discontinuity) are hardly detectable. Models of D'' like PWDK and PGLE remain unable to match the **four slowness data sets at the same time.** On the contrary, the PREM (or iasp91) reference model is in good agreement with all of them; however, it cannot account for the PdP observations of the previous sections. A D'' structure including reflectors of regional extension at its top would perhaps remove this contradiction. We point out an alternative explanation: the PREM and D'' models with a discontinuity both predict correct P-wave first-arrival times. The drop in velocity gradient about 200 km above the core–mantle boundary could therefore result from trying to fit the traveltimes with a model with **no** discontinuity. Since a discontinuity at the top of D'' is required in order to explain the secondary arrivals observed in different regions, this suggests that this discontinuity may be a global feature.

CONCLUSION

We have investigated the structure of the D'' layer at the base of the mantle beneath northern Siberia, on the 100–1000 km scale, using the french short-period L.D.G network in France. In the 75–82° distance range, intermediate arrivals between the P and PcP waves are observed, and clearly identified as waves reflected on a lower mantle discontinuity about 300 km above the core–mantle boundary. This extends the observations of Weber & Davis (1990), Weber (1993), and Gaherty & Lay (1992) to the north and northwest. It also confirms the prediction of Weber & Körnig (1992), in a statistical work on ISC bulletins, that northern Siberia is a good candidate for such studies.

A deconvolution technique, where the data are deconvolved from a source-time function derived from the data, has been extensively used. Record sections of deconvolved data from different earthquakes have been constructed, which show the PdP-wave move out with distance remarkably well, over more than 5°. The analysis of the T_{PdP}–T_P traveltime residuals shows the existence of lateral variations in the structure of the 'Lay discontinuity'. Further evidence of the signature of a classical triplication pattern is searched. **In the hypothesis that the discontinuity may extend further south, in northern Siberia,** the D'' structure is investigated in the 88°–93° distance range, well beyond the theoretical cross-over. It supports the existence of rather large gradients above the discontinuity. Finally, the hodochrones of the first P arrival are used, as an additional constraint on the gradient above the discontinuity. Four reference focus depths have been chosen. Smooth lower mantle models like PREM, and models with a 'Lay discontinuity' like PGLE and PWDK, match the p-Delta distribution well, **before** and **after** the 82°–85° cross-over distance range (55 km data set). For the 98, 130 and 575 km depths, the cross-over distance range is sampled; the PREM model still matches the slowness data well, but the PGLE and PWDK models are no longer accurate. The impossibility for PREM, unlike models like PGLE or PWDK, to predict secondary arrivals between the P and PcP waves between 75° and 82°, but its ability to match the first P-wave propagation branch, suggests that D'' may be a global feature around the globe. A further indication is the fact that the PdP wave may be detectable only at some stations of a network, even at the same distance range. The absence of observation should perhaps not be interpreted systematically as an absence of reflector, or as the effect of crustal reverberation beneath the stations, but also as the effect of lateral variations of the topography or thickness of the reflector.

ACKNOWLEDGMENTS

We are thankful to the people who run the L.D.G. network, and in particular to Bernard Massinon and Jean-Louis

Plantet, for making the data available to us. We thank Michael Weber and Thorne Lay for useful discussions and remarks, and Michael Weber for the careful review of our paper. They also provided several preprints prior to publication. We are grateful to Christophe Vigny for making drawing software available to us. This work was supported by the 'Centre National de la Recherche Scientifique' (INSU/IST Tomography). E.N.S PARIS—Département T.A.O.

REFERENCES

Baumgardt, D. R., 1989. Evidence for a *P* wave velocity anomaly in *D"*, *Geophys. Res. Lett.*, **16,** 657–661.

Chapman, C. H., 1976. A first motion alternative to geometrical ray theory, *Geophys. Res. Lett.*, **3,** 153–156.

Chapman, C. H. & Orcutt, J. A., 1985. The computation of body wave seismograms in laterally homogeneous media, *Rev. Geophys.*, **23,** 105–163.

Chapman, C. H., Chu, J.-Y. & Lyness, D. G., 1988. The WKBJ Seismogram Algorithm, in *Seimological Algorithms, Computational methods and Computer Programs,* pp. 47–74, ed. Doornbos, D., Academic Press, London.

Dey-Sarkar, S. K. & Chapman, C. H., 1978. A simple method for the computation of body wave seismograms, *Bull. seism. Soc. Am.*, **68,** 1577–1593.

Dziewonski, A. M. & Anderson, D. L., 1981. Preliminary reference earth model, *Phys. Earth planet. Inter.*, **25,** 297–356.

Gaherty, J. B. & Lay, T., 1992. Investigation of laterally heterogeneous shear velocity structure in *D"* beneath Eurasia, *J. geophys. Res.*, **97,** 417–436.

Garnero, E., Helmberger, D. & Engen, G., 1988. Lateral variations near the core–mantle boundary, *Geophys. Res. Lett.*, **15,** 609–612.

Haddon, R. A. W. & Buchbinder, G. G. R., 1986. Wave propagation effects and the earth's structure in the lower mantle, *Geophys. Res. Lett.*, **13,** 1489–1492.

Houard, S. & Nataf, H. C., 1992. Further evidence for the 'Lay discontinuity' beneath Northern Siberia and the North Atlantic from short-period *P*-waves recorded in France, *Phys. Earth planet. Inter.*, **72,** 264–275.

Lay, T., 1989. Structure of the core–mantle transition zone: a chemical and thermal boundary layer, *EOS, Trans. Am. geophys. Un,* **70,** 49.

Lay, T. & Helmberger, D. V., 1983a. A shear velocity discontinuity in the lower mantle, *Geophys. Res. Lett.*, **10,** 63–66.

Lay, T. & Helmberger, D. V., 1983b. A lower mantle S-wave triplication and the shear velocity structure of *D"*, *Geophys. J. R. astr. Soc.*, **75,** 799–837.

Richards, P. G., 1976. On the adequacy of plane-wave reflection/transmission coefficients in the analysis of seismic body waves, *Bull seism. Soc. Am,* **66,** 701–717.

Schlittenhardt, J., Schweitzer, J. & Müller, G., 1985. Evidence against a discontinuity at the top of *D"*, *Geophys. J. R. astr. Soc,* **81,** 295–306.

Vandecar, J. C. & Crosson, R. S., 1990. Determination of teleseismic relative phase arrival times using multichannel cross-correlation and least squares, *Bull. seism. Soc. Am,* **80,** 150–169.

Weber, M., 1990. Subduction zones—their influence on traveltimes and amplitudes of *P*-waves, *Geophys. J. Int.*, **101,** 529–544.

Weber, M., 1993. *P*- and *S*-wave reflections from anomalies in the lowermost mantle, *Geophys. J. Int.*, **115,** 183–210.

Weber, M. & Davis, J. P., 1990. Evidence of a laterally variable lower mantle structure from *P*- and *S*-waves, *Geophys. J. Int.*, **102,** 231–255.

Weber, M. & Körnig, M., 1992. A search for anomalies in the lowermost mantle, *Phys. Earth planet. Inter.*, **73,** 1–28.

Young, C. J. & Lay, T., 1987. The core–mantle boundary, *Ann. Rev. Earth planet. Sci.*, **15,** 25–46.

Young, C. J. & Lay, T., 1990. Multiple phase analysis of the shear velocity structure in the *D"* region beneath Alaska, *J. geophys. Res.*, **95,** 17385–17402.

Zhang, J. & Lay, T., 1984. Investigation of a lower mantle shear wave triplication using a broadband array, *Geophys. Res. Lett.*, **11,** 620–623.

APPENDIX

The following procedure has been followed to derive 1-D models based on residual-time data sets: the PREM reference model has been perturbed at the base of the mantle, below a radius of 4070 km (like in the PWDK and PGLE models). As a matter of fact, direct *P* waves do not travel below that radius, for epicentral distances shorter than 70°. Then, the upper gradient value is incremented, in regular steps, from zero to the PREM value. For each value, a mean *P*-velocity jump at the discontinuity is chosen (usually between 2 and 3 per cent) and the depth of the discontinuity for which theoretical residuals match the data best is obtained by dichotomy. For both residual-time tendencies, it has been quite clear that low upper gradient values (like in PWDK) could be rejected. Their corresponding *PdP* residual slownesses were far too small to match the data.